PHYSICAL REVIEW D **78,** 109901(E) (2008)

Erratum: Nonlinear perturbation theory with halo bias and redshift-space distortions via the Lagrangian picture [Phys. Rev. D 78, 083519 (2008)]

Takahiko Matsubara

(Received 17 October 2008; published 4 November 2008)

DOI: 10.1103/PhysRevD.78.109901 PACS numbers: 98.80.−k, 95.35.+d, 95.36.+x, 98.65.−r, 99.10.Cd

Equations (55), (58), and (59) should be replaced by

$$\langle F^{(n)}_{M_1}\rangle = \frac{(-1)^n}{g(\nu_1)}\left(\frac{\partial}{\partial\delta_1}\right)^n g(\nu_1) = \frac{(-1)^n {\nu_1}^n}{{\delta_1}^n g(\nu_1)}\frac{\partial^n g(\nu_1)}{\partial {\nu_1}^n}, \tag{55}$$

$$\langle F''\rangle = \frac{1}{{\delta_c}^2(z)}\left[q^2\nu^4 - 3q\nu^2 + \frac{2p(2q\nu^2+2p-1)}{1+(q\nu^2)^p}\right], \tag{58}$$

$$\langle F^{(n)}\rangle = \frac{(-1)^n}{{\delta_c}^n(z)}\frac{\int_{M_1}^{M_2}\nu^n\frac{d^n g}{d\nu^n}\frac{d\ln\sigma}{dM}\frac{dM}{M}}{\int_{M_1}^{M_2} g(\nu)\frac{d\ln\sigma}{dM}\frac{dM}{M}}. \tag{59}$$

The above changes do not affect other equations and conclusions of the paper. Figures 1–5 slightly change in detail but not in qualitative manner (see new versions of Figs. 1–5).

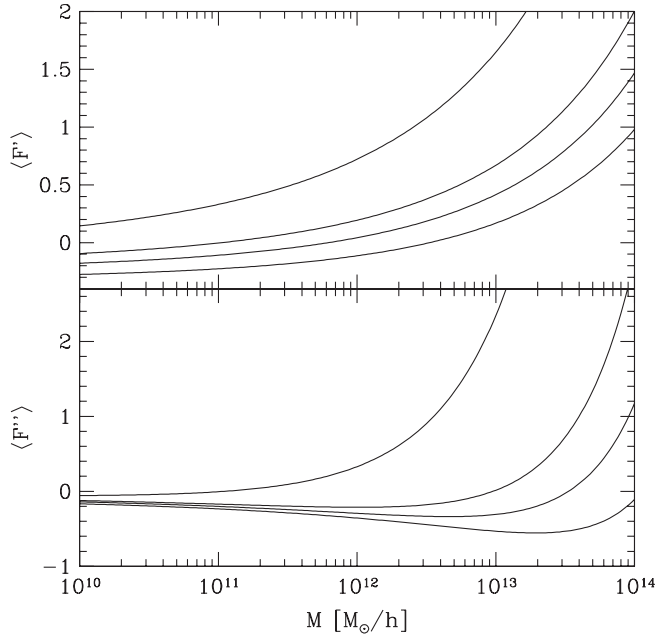

FIG. 1. Local Lagrangian bias parameters $\langle F'\rangle$ and $\langle F''\rangle$ as functions of halo mass. Different curves correspond to different redshifts ($z = 0, 0.5, 1, 3$ from bottom to top in each panel).

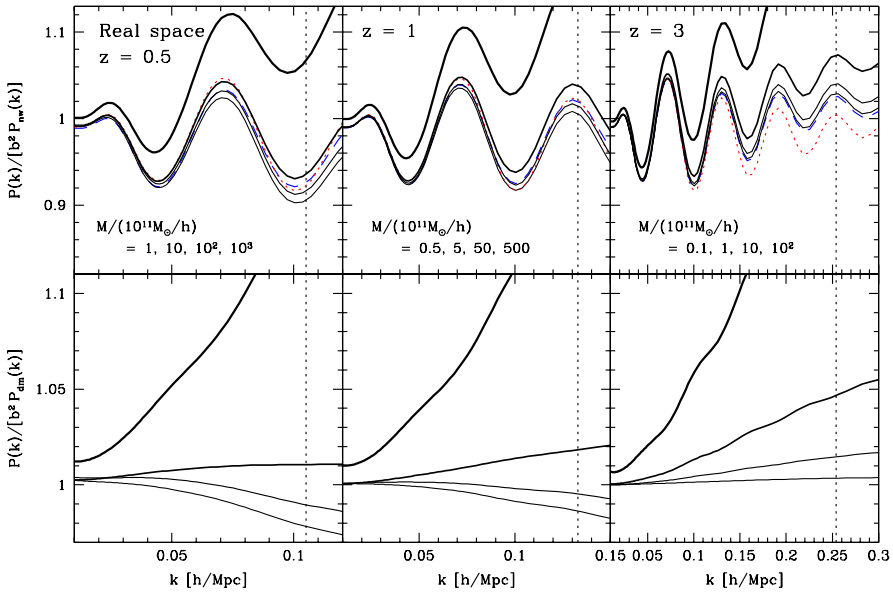

FIG. 2 (color online). Dependencies on halo mass and redshift of the nonlinear power spectrum in real space. In the top panels, each power spectrum is divided by a smoothed, no-wiggle linear power spectrum $P_{\rm nw}(k)$ [58] and by a squared linear bias factor b^2. Values of redshifts and halo masses are shown in each panel. Solid lines: Nonlinear power spectra of halos with different masses with increasing order from thinner to thicker lines; dotted lines: linear theory; dashed lines: nonlinear power spectra of dark matter. In the bottom panels, halo power spectra are divided by corresponding mass power spectra and by the squared linear bias factor, presenting the scale dependence of halo bias. Vertical short-dashed lines correspond to the scale $k_{\rm NL}/2$ to indicate the validity range $k < k_{\rm NL}/2$, where our result is expected to be accurate within a few percent.

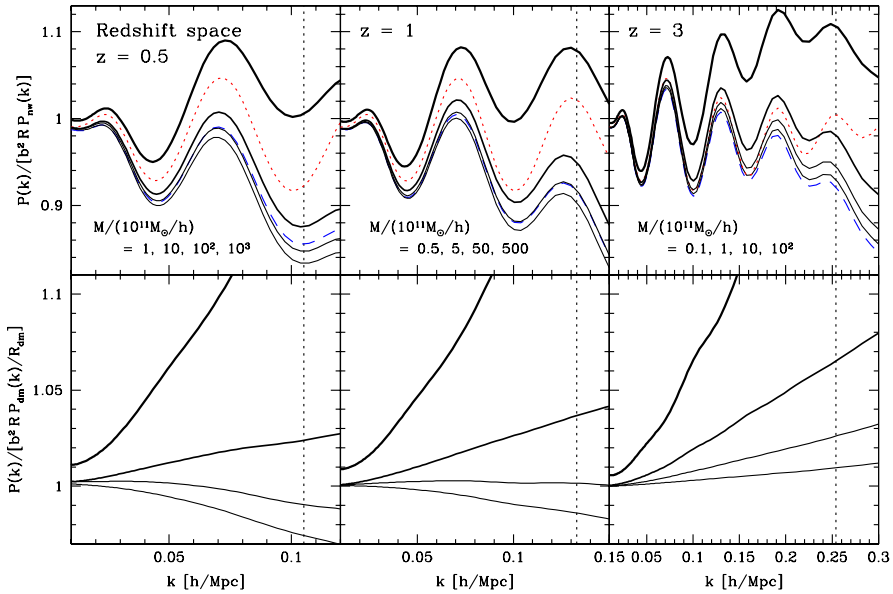

FIG. 3 (color online). Same as Fig. 2 but in redshift space. Spherically averaged power spectra are plotted. Linear redshift-space enhancement factor $R = 1 + 2\beta/3 + \beta^2/5$ is also scaled out.

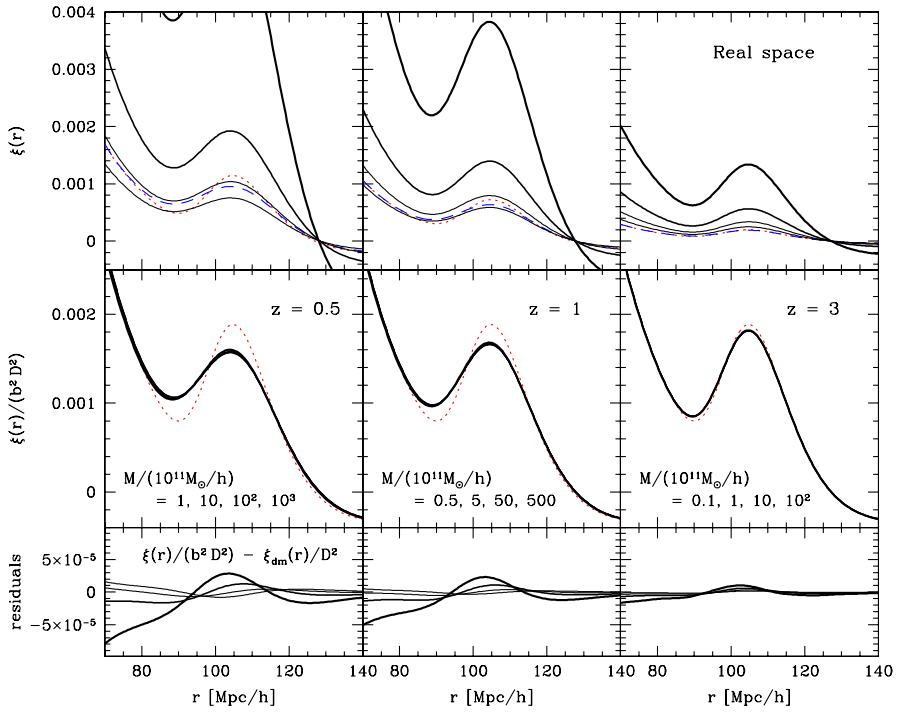

FIG. 4 (color online). Dependencies on halo mass and redshift of the nonlinear correlation function in real space. Correlation functions with a fixed redshift and with different halo masses are presented in each column. Mass of the halo varies in increasing order from thinner to thicker solid lines. Dotted lines correspond to the prediction of linear theory, and dashed lines correspond to nonlinear correlation functions of dark matter. In the top rows, the bare values of correlation function are plotted. In the middle rows, the correlation functions are normalized by linear bias factors and linear growth factors. In the bottom rows, residual values in the normalized correlation function of halos (plotted in middle rows), relative to that of dark matter, are plotted.

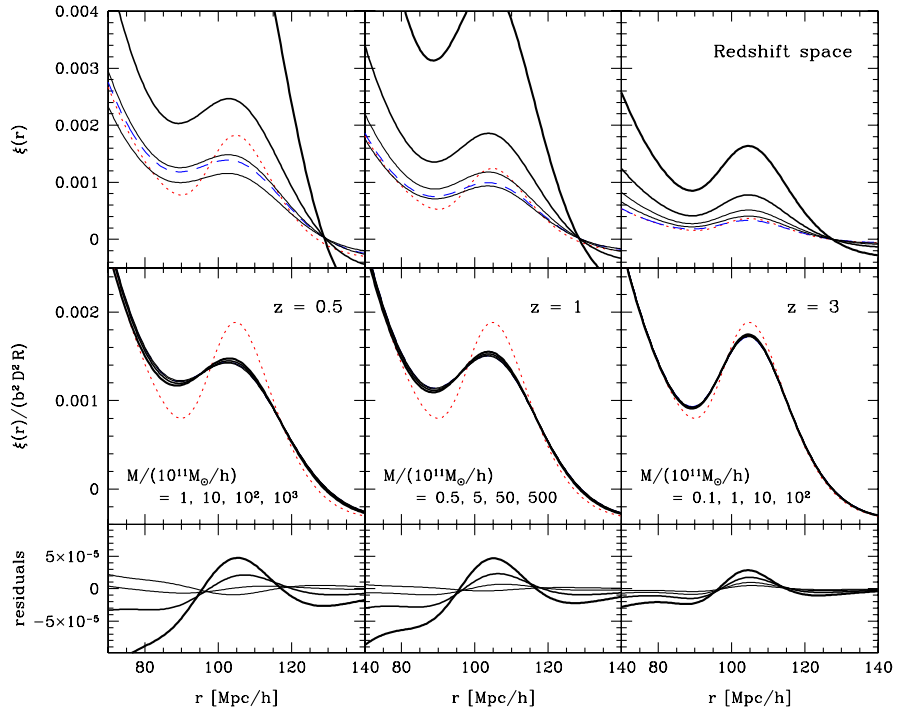

FIG. 5 (color online). Same as Fig. 4 but in redshift space. Spherically averaged correlation functions are plotted. Linear redshift-space enhancement factor R is also scaled out.